



1 **Transport behavior displayed by water isotopes and**
2 **potential implications for assessment of catchment**
3 **properties**

4

5 Dan Elhanati¹, Erwin Zehe², Ishai Dror¹, and Brian Berkowitz¹

6

7 ¹ Department of Earth and Planetary Sciences, Weizmann Institute of Science, Rehovot,
8 Israel

9 ² Institute of Water Resources and River Basin Management, Karlsruhe Institute of
10 Technology (KIT), Karlsruhe, Germany

11

12

13 **Correspondence:** Brian Berkowitz (brian.berkowitz@weizmann.ac.il)

14



15 **Abstract.**

16 Measurements of water isotopes are used routinely to estimate water transit time
17 distributions and aquifer storage thickness in catchments. Water isotopes (e.g., $D_2O/H_2^{18}O$)
18 are generally considered to behave identically to water molecules (H_2O); they are thus often
19 considered fully representative of water movement and preferred over inert chemical
20 tracers for catchment assessment purposes. However, laboratory-scale measurements
21 presented here show that water isotopes exhibit transport behavior that is essentially
22 identical to that of inert chemical tracers. The resulting measurements are then interpreted
23 quantitatively, focusing on a comparative assessment of apparent mean water and mean
24 tracer velocities, and the applicability of Fickian and non-Fickian (anomalous) transport
25 models. For both water isotopes and inert chemical tracers, the measured mean tracer
26 velocity is not necessarily equal to the apparent mean water velocity. It is thus critical to
27 recognize this inequality when estimating catchment properties. For example, accounting
28 for anomalous transport of water isotopes can significantly reduce overall estimates of
29 aquifer storage thickness over an entire watershed.



30 1 Introduction

31 River catchments and streamflow play a pivotal role in water resources management
32 (Sivapalan, 2018). A catchment represents a three-dimensional hydrological unit
33 delineated by a watershed boundary, where precipitation is partly stored in the subsurface
34 and partly released as evapotranspiration or runoff components, ultimately feeding
35 streamflow. While the catchment water balance controls generation of streamflow
36 amounts, catchments can be also regarded in analogy to chemical reactors (Grathwohl et
37 al., 2013). Streamflow chemistry and contaminant fate are thus essentially controlled by
38 the interplay of transport velocities and, in the case of reactive species, reaction rates of
39 chemicals traveling through the catchment (Grathwohl et al., 2013; Berkowitz et al., 2016;
40 Sternagel et al., 2021).

41 Natural catchments comprise inherent structural complexities above and below the land
42 surface, which lead to heterogeneous spatial and temporal distributions of flow velocities.
43 Accurately describing travel times in catchments is thus by no means straightforward
44 (McDonnell et al., 2010). Travel (or transit) time distribution (TTDs) of *water*, defined as
45 the durations water molecules require to traverse the catchment from rainfall to stream, are
46 often regarded as a key metric for inferring streamflow chemistry (e.g., McGlynn et al.,
47 2003; Weiler et al., 2003; Hrachowitz et al., 2013; Rodriguez et al., 2021; Benettin et al.,
48 2022). A water TTD, and in particular the mean of the water TTD (from which one can
49 infer the mean water velocity), is often used, for example, to estimate water storage and
50 aquifer thickness in a catchment. However, it is difficult to uniquely define or determine a
51 water TTD: clearly, one cannot directly measure the velocity of water molecules in an
52 advective field.

53 More broadly, TTDs, *sensu lato* – e.g., TTDs of water, chemicals, and momentum –
54 may represent different transport processes, which differ strongly with respect to the
55 underlying mechanism and can also be time-dependent and substance-specific (Rinaldo et
56 al., 2011). A common approach for inferring *water* TTDs of a catchment involves applying
57 measurements of a tracer pulse transported by the water as input for a transport model. The
58 normalized breakthrough curve of a unit mass input of the tracer thus corresponds to the
59 tracer TTD, reflecting the distribution of fluid velocities and subscale diffusive mixing of
60 tracer molecules between the flow lines (Simmons, 1982; Jury and Sposito, 1986). In this



context, models that describe various catchment transport processes are used to estimate water TTDs from tracer breakthrough curves (e.g., McGuire and McDonnell, 2006; Bowers et al., 2020; Sternagel et al., 2022; Wienhoefer et al., 2009; McDonnell et al., 2010; Lischeid et al., 2000).

While measurements of any inert chemical tracer transported by the flow of water in a catchment are often assumed to be suitable for inferring water TTDs, many studies focus on use of ratios of isotopic tracers of the water molecule itself (i.e., the isotopologues H_2^{18}O , $^2\text{H}_2\text{O}$, $^3\text{H}_2\text{O}$), because these molecules are considered to behave identically to H_2O and they often enter the catchment naturally through rainfall (e.g., McDonnell and Beven, 2014; Rodriguez et al., 2021; Sternagel et al., 2022; Weiler et al., 2003; Aquilina et al., 2006; Koeniger et al., 2010). They are therefore regarded as an optimal tracer of water, compared to other chemical tracers (McGuire and McDonnell, 2006).

The above brief survey highlights the wide range of interpretations and methods related to TTD assessment, particularly to estimates of *water* TTDs. Motivated by the literature discussed above, the study here focuses on a frequently invoked, key assumption, namely that isotopic tracers of the water molecule itself behave identically to H_2O (with only slightly different diffusion coefficients because of slightly different molecular weights) and can therefore be used to infer the true mean water velocity and residence time in a porous domain. For this purpose, water isotope tracer transport in a critical subset of a full catchment – namely, the fully water-saturated domain – is examined. Breakthrough curves of a water isotope and an inert chemical tracer are measured in macroscopically 1D porous medium columns; the resulting curves are compared and subsequently interpreted quantitatively. A fundamental question is thus studied: What are the implications of using water isotopes as tracers, as compared to inert chemical tracers, in terms of defining a water TTD and its mean?

2 Methods

A laboratory-scale experimental setup was constructed to compare the transport behavior of inert chemicals to the transport behavior of water isotopes. This setup aimed to examine flow and transport in a controlled saturated porous medium, allowing the measurement and comparison of the tracer (Br) and a water isotope tracer (water containing



92 a higher D_2O/H_2O ratio than commonly found in nature) in a flow regime which exhibits
93 anomalous transport.

94 In a previous study, Elhanati et al. (2023) examined the transport behavior of an inert
95 chemical tracer (Gd) in porous medium columns, under time-dependent velocity conditions
96 in a macroscopically 1D flow regime. The same experimental setup was adapted for this
97 study as it consistently showed anomalous transport for different flow rates and porous
98 medium arrangements. The setup consisted of three vertical columns measuring 100 cm in
99 length with an internal radius of 1.4 cm, packed with a fully water-saturated porous medium
100 composed of clean quartz sand grains, and with water and tracer injected from below. First,
101 three effectively (macroscopically) homogeneous porous medium columns (Columns I-III)
102 were packed uniformly with sand having an average grain size of 1.105 mm (mesh size
103 12/20), and porosity of 0.38. Subsequently, the three columns were cleaned, and each was
104 packed with an alternating pattern of three different sand sizes (Columns IV-VI) to produce
105 a heterogeneous porous medium (see Elhanati et al., 2023 for a full description of the
106 experimental setup). Elhanati et al. (2023) reported that both packing configurations (i.e.,
107 homogeneous and heterogeneous) displayed long tailing in the Gd breakthrough curves
108 and other behavior indicative of anomalous transport.

109 Three solutes were used for this study: (1) NaBr salt, an inert tracer used as a benchmark,
110 with an initial concentration of 10 ppm Br; (2) D_2O , with an initial concentration of 10,000
111 ppm D; (3) A combination of both solutes (NaBr and D_2O). Repeating the experiments
112 with a combined solute of D_2O enriched water and Br allowed comparison of the resulting
113 breakthrough curves. Although an interaction of the two tracers was not expected, the
114 experiment was repeated with only the D_2O for validation. Each experiment was conducted
115 simultaneously in the three columns, starting with a short solute injection before switching
116 to double-distilled water flow for the rest of the experiment. Samples were collected at the
117 column outlets using a fraction collector.

118 First, experiments were conducted in a homogeneous medium using coarse-grained sand
119 for the three solutes mentioned above (experiment sets A1: NaBr+ D_2O , A2: D_2O , and A3:
120 NaBr, respectively; $Q = 1.0$ mL/min). Next, the homogeneous experiments were repeated
121 with the combined NaBr and D_2O solute with a higher flow velocity, namely double
122 volumetric discharge (experiment set A1_{fast}: NaBr+ D_2O ; $Q = 2.0$ mL/min), to test for



consistency in different flow conditions. Subsequently, two sets of experiments in a heterogeneous medium for the slow (experiment set B1: NaBr+D₂O) and fast (experiment set B1_{fast}: NaBr+D₂O) flow conditions were performed. See Table 1 for a summary of the experiments. To add perspective, a representative Peclet number (Pe) for the experimental set-up can be estimated. Here, $Pe = L\bar{v}_w/D$, where L is a characteristic length, chosen here as the average grain size diameter ($L = 0.11$ cm), \bar{v}_w is the average local flow velocity, and D is a mass diffusion coefficient ($D = 2 \times 10^{-5}$ cm²/s, representative of typical inert anionic tracers like bromide). For the uniformly packed sand columns with $Q = 1.0$ mL/min, $\bar{v}_w = 7.1 \times 10^{-3}$ cm/s (see calculation in Sect. 3.2), so that $Pe \approx 39$.

Table 1. Set-up and conditions of column experiments.

Experiment	Packing	Flow Rate	Solute
A1	Uniformly packed sand (Columns I, II, III)	1.0 mL/min	NaBr+D ₂ O
A2	uniformly packed sand (Columns I, II, III)	1.0 mL/min	D ₂ O
A3	Uniformly packed sand (Columns I, II, III)	1.0 mL/min	NaBr
A1 _{fast}	Uniformly packed sand (Columns I, II, III)	2.0 mL/min	NaBr+D ₂ O
B1	Alternating pattern of three different sand sizes (Columns IV, V, VI)	1.0 mL/min	NaBr+D ₂ O
B1 _{fast}	Alternating pattern of three different sand sizes (Columns IV, V, VI)	2.0 mL/min	NaBr+D ₂ O

134

Water samples were measured by Inductively Coupled Plasma-Mass Spectrometry (ICP-MS; Agilent). The ICP-MS ionizes the samples and detects the presence of specific atomic masses, which allows the determination of the concentration of the Br and D at the column outlet throughout the experiment. While isotopes of light elements are not readily measurable by ICP-MS due to low ionization efficiency and spectral interference, it is possible to measure deuterium-containing polyatomic species (e.g., ArD⁺) as an accurate



proxy for D analysis (Galbács et al., 2020). In excess of H₂O, D₂O rapidly converts to HDO in equilibrium ($D_2O + H_2O \rightleftharpoons 2HDO$), which is linearly correlated to the measurable ArD⁺ ion in the plasma. While the measured Br background concentration is below the instrument detection limit, the double distilled water applied in the experiment comprises a naturally occurring D₂O/H₂O ratio. The background concentration was subtracted from the results presented to show the breakthrough of the Br and D₂O solutes over their naturally occurring background concentration.

3 Results and discussion

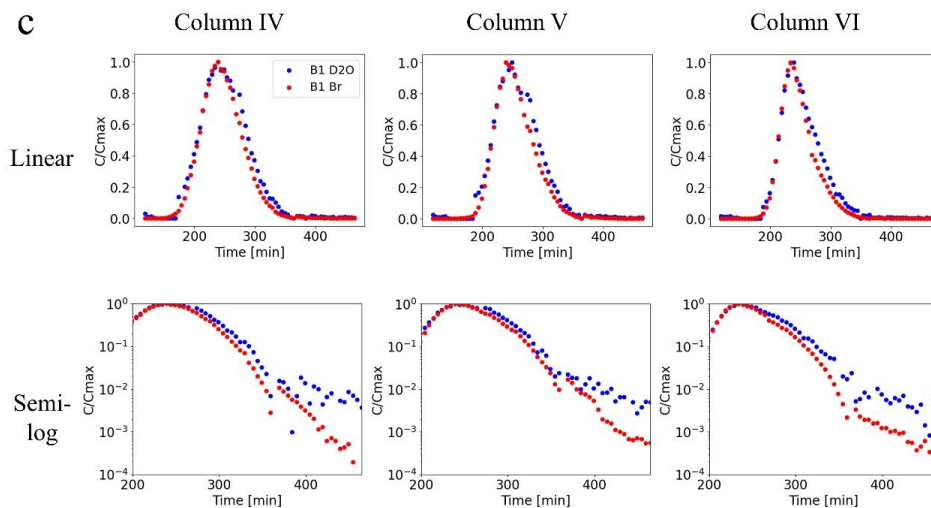
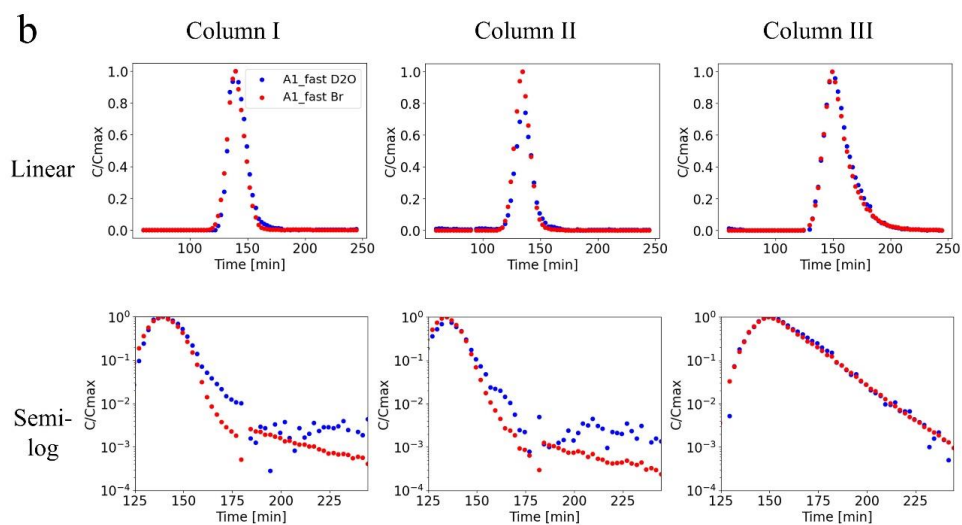
3.1 Comparison of Br and D₂O breakthrough curves

The slow-flow homogeneous porous medium experiments show similar behavior for the enriched-deuterium water and the bromide tracer (Fig. 1a). Both signals show a similar breakthrough curve, as demonstrated by the onset and length of the breakthrough measured at the outlet. This finding is consistent for the bromide and D₂O when injected as a single chemical species or when combined in a single experiment. This coupling establishes the similar behavior of the two chemical species, independent of a dynamic resulting from the simultaneous injection. This finding is apparent for all three columns, which show the same behavior in different packing arrangements. Column III, in particular, displayed longer tails of the breakthrough curves, consistently for both the Br and the D₂O. This can be seen, in particular, in the semi-log scale which allows a focus on the long-tailed behavior. The faster flow experiments also showed consistency of this finding across the three columns (Fig. 1b). The heterogeneous porous medium experiments show longer tails compared to the homogeneous porous medium experiments, for both the slow flow and high flow experiments. For both flow scenarios, the bromide tracer and D₂O water displayed similar breakthrough curves for each column (Figs. 1c and 1d). The various replicate experiments shown in Fig. 1 illustrate natural variability, which is exhibited particularly in the behavior of the long-time tails for each specific column and flow rate.

The results of both the heterogeneous and homogeneous column experiments, and for different flow rates, show that water isotopes behave similarly to inert chemical tracers. This finding is discussed in detail in Sect. 3.2 and Sect. 3.3. In both the homogeneous and

177

178



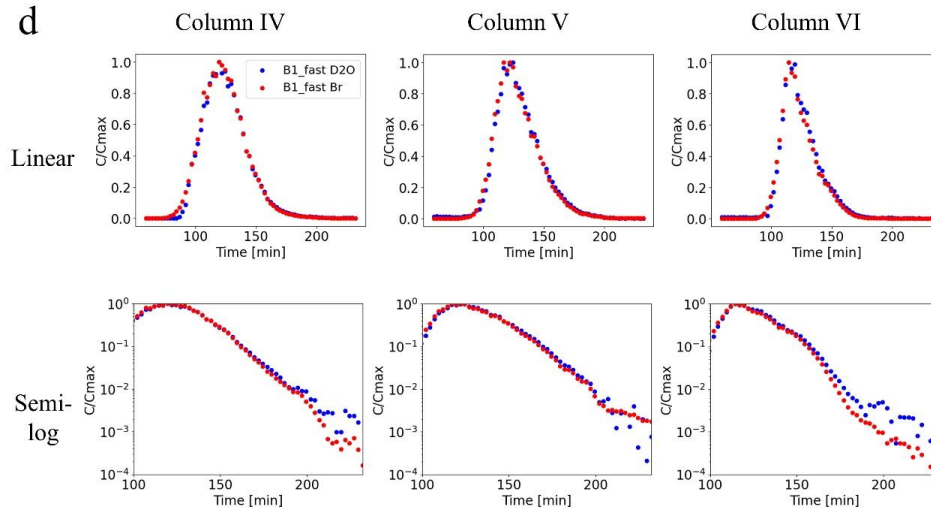


Figure 1. Breakthrough curves (A1, B1: D₂O+Br; A2: D₂O; A3: Br) for the three homogeneous and the three heterogeneous porous medium columns in linear scale (top row) and semi-log scale (bottom row). (a) homogeneous slow-flow experiments (A1: NaBr+D₂O, A2: D₂O, A3: NaBr); (b) homogeneous fast-flow experiments (A1_{fast}: NaBr+D₂O); (c) heterogeneous slow-flow experiments (B1: NaBr+D₂O); (d) heterogeneous fast-flow experiments (B1_{fast}: NaBr+D₂O). D₂O concentrations at the tailing end of the breakthrough are generally slightly higher than Br concentrations, because the naturally occurring D₂O/H₂O ratio fluctuates around the measured background value. Note the different time scales between experiments.

3.2 Water and tracer transport in a fully water-saturated porous media: a Gedanken experiment

While one cannot directly measure velocity of water molecules, an *apparent average water velocity*, \bar{v}_w , which represents an average macroscopic value over the entire medium, is commonly determined by use of Darcy's law. In a macroscopically 1D column, for example, \bar{v}_w can be determined by the simple relation $\bar{v}_w = Q/nA$, where Q is fixed volumetric discharge, n is an effective porosity (e.g., determined by comparing weights of a sand or rock core sample under dry and then water-saturated conditions), and A is the cross-sectional area of flow.

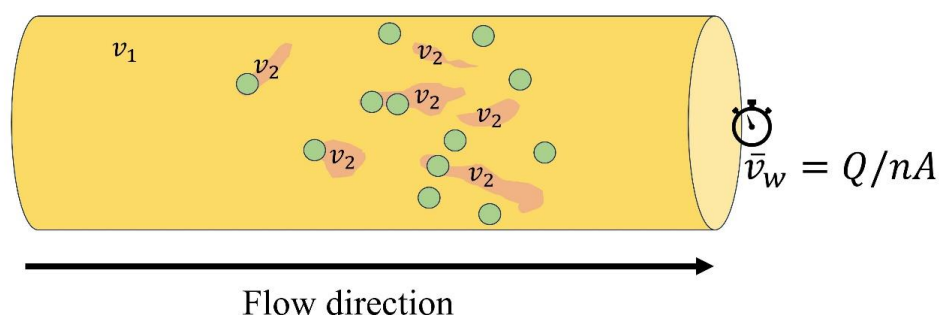
A critical question then arises: is the average velocity of an inert chemical tracer, \bar{v}_T , identical to that of the apparent average water velocity, \bar{v}_w ? In principle, the answer is, in



203 general, no (i.e., $\bar{v}_w \neq \bar{v}_T$), unless the domain is perfectly homogeneous over the length
204 and/or time scales of measurement (e.g., Cortis et al., 2004).

205 A Gedanken experiment is useful to visualize this important difference. In a fully water-
206 saturated porous column containing pore-scale heterogeneities, or very small-scale, lower
207 permeability inclusions embedded in the column, the flow and transport are
208 macroscopically 1D (Fig. 2). The behavior of the water and the migration of an inert tracer,
209 such as Br^- , can be determined theoretically. By estimating the porosity and cross-sectional
210 area of flow through the column, and for a fixed Q , \bar{v}_w can be calculated using Darcy's law,
211 and the mean travel time of water through the column can be estimated by dividing the
212 column length by \bar{v}_w . Measuring the Br^- ions, however, will expectedly yield a different
213 result: if a pulse of X Br^- ions is injected into the column, Y Br^- ions may reach the
214 inclusions and remain there for a very long time. Estimation of the mean velocity, \bar{v}_T , of
215 the Br^- ions at the column outlet would thus result in lower velocity compared to the
216 apparent mean water velocity, due to the slow-moving ions (i.e., a long-tail in the tracer
217 breakthrough measurement).

218



219

220 **Figure 2.** Conceptual macroscopically 1D flow through a 1D porous medium column with
221 a mean velocity (\bar{v}_1) containing (very small-scale or pore-scale) lower velocity inclusions
222 (\bar{v}_2). The Br^- ions injected as a pulse into the column are marked with green circles.
223 Calculation of the apparent mean water velocity (\bar{v}_w) at the column outlet will yield a
224 higher velocity than the actual velocity of the transported Br^- ions due to the lower
225 velocities experienced by some Br^- ions in the inclusions.

226

227 This Gedanken experiment leads to the expected conclusion that the mean velocity of
228 the chemical tracer does not necessarily represent the apparent mean water velocity, due to



229 even small-scale mobile and immobile zones in the medium. However, it is also clear that
230 the origin of the measured behavior of the inert tracer is the direct result of the measurement
231 process. One can replace the Br^- ions in the above example with water isotopes and reach
232 the same result: some of the tagged water molecules will reach the inclusions and the
233 estimated mean tracer velocity \bar{v}_T will be slower than the apparent mean water velocity
234 \bar{v}_w . The act of tagging water effectively changes a water molecule to act as a “non-water”
235 tracer, in the context of breakthrough measurements; in other words, the measured velocity
236 represents the mean velocity of a tracer (be it a water isotope or an inert chemical), rather
237 than the apparent mean velocity of the water.

238

239 3.3 Quantification of transport behavior

240 It is important to recognize the inherent difference between \bar{v}_w and \bar{v}_T when quantifying
241 tracer transport in a fully water-saturated porous medium. In a macroscopically one-
242 dimensional domain, the apparent mean water velocity \bar{v}_w does not represent the actual
243 travel times of all water molecules through the medium, but rather an average macroscopic
244 value over the entire medium. On the other hand, an inert tracer transported by the water is
245 subjected to advection and hydrodynamic dispersion, as well as to subscale diffusive
246 mixing. As the chemical tracer is transported through the medium, it displays a distribution
247 of velocities which represents a fingerprint of the heterogeneous flow paths. Therefore, the
248 transport of a tracer inherently reflects a distribution of velocities for which \bar{v}_T represents
249 the mean.

250 With this understanding, how does one interpret and quantify experimental results such
251 as those discussed in Sect. 3.1? In an effectively (macroscopically, continuum-level)
252 homogeneous porous medium, the tracer particles can in essence display Fickian dispersion
253 and $\bar{v}_w = \bar{v}_T$ (Berkowitz et al., 2006). In this situation, the classical 1D form of the
254 advection-dispersion equation (ADE) for steady-state flow can be applied to quantify the
255 transport dynamics, $\partial C / \partial t = -v \partial C / \partial x + D^* \partial^2 C / \partial x^2$, where the by velocity v is by
256 definition based on \bar{v}_w and D^* is a dispersion coefficient. However, in many cases, the
257 velocity distribution often gives rise to non-Fickian (or anomalous) transport, which can
258 be manifested by, e.g., the occurrence of long tails in measured breakthrough curves (e.g.,



259 Cortis et al., 2004; Berkowitz et al., 2006). Thus, the effect of anomalous transport may be
260 significant for mean TTD estimation, which might differ substantially from the apparent
261 mean water velocity; this is discussed in Sect. 3.4.

262 Here, the continuous time random walk framework (CTRW) was used to interpret
263 measured breakthrough curves (Berkowitz et al., 2006) such as shown in Fig. 1. The CTRW
264 represents a continuum-scale, ensemble average behavior relevant to the interpretation of
265 these macroscopically 1D column experiments; it is especially suitable for this task because
266 it inherently employs \bar{v}_T in its formulation. Solutions based on CTRW have been shown to
267 yield a good description of non-Fickian transport scenarios (Dentz et al., 2008, 2018, 2023;
268 Edery et al., 2015; Bijeljic et al., 2011, 2013; Nissan and Berkowitz, 2019; Goepfert et al.,
269 2020).

270 In a CTRW particle tracking (PT) formulation, applied here, probability density
271 functions stochastically define particle transitions in space and time (see Elhanati et al.,
272 2023 and Nissan et al., 2017 for a complete mathematical description). A truncated power
273 law distribution is assigned for the temporal probability density function, defined with the
274 exponent β , which is a measure of the non-Fickian nature of the transport (Nissan et al.,
275 2017). A power law exponent of $\beta > 2$ implies Fickian, or essentially Fickian, behavior for
276 which an ADE solution is generally applicable (Berkowitz et al., 2006); $\beta < 2$ is a descriptor
277 of non-Fickian transport. The first spatial moment of the chemical species plume in the
278 flow direction, v_ψ , is defined as the mean particle velocity and is therefore applied herein
279 as the mean tracer velocity, \bar{v}_T . It is noted that the breakthrough curves from the
280 experiments presented here were expected to display anomalous transport based on
281 experiments and analysis reported previously by Elhanati et al. (2023). Anomalous
282 transport even in macroscopically homogeneous porous media arises because of subtle,
283 residual pore-scale disorder effects, with diffusion into pore-scale stagnant regions that can
284 lead to a wide (power law) distribution of travel times (Cortis et al., 2004; Berkowitz et al.,
285 2006).

286 Two key characters are assessed in this context, focusing on a representative
287 breakthrough curve: the mean velocity of the D₂O tracer and the nature of the long tails in
288 the breakthrough curves. As an example, the slow flow homogeneous porous medium D₂O
289 (A1) dataset was interpreted using the CTRW-PT formulation discussed above. An



290 approximate fit to the data yielded a power law exponent of $\beta \approx 1.84$ (Fig. 3), which is
291 indicative of anomalous transport.

292 Moreover, the CTRW-PT simulation yielded a mean tracer velocity of $\bar{v}_T = 5.8 \times 10^{-3}$
293 cm/s. In sharp contrast, for this experiment, the apparent mean water velocity can be
294 directly determined as $\bar{v}_w = 7.1 \times 10^{-3}$ cm/s for the experiment parameters ($Q = 1.0$ mL/min,
295 $n = 0.38$, and $A = 6.16$ cm²). Clearly, $\bar{v}_w \neq \bar{v}_T$. Figure 3 also shows two representative fits
296 of the data using a 1D solution of the classical ADE. Here, using the value of $\bar{v}_w = 7.1 \times$
297 10^{-3} cm/s, which according to the theory underlying the Fickian-based ADE is the relevant
298 velocity, the solution is seen to strongly over-estimate the advance of the peak, and to be
299 unable to capture the long-time tailing. Furthermore, even if the mean velocity in the ADE
300 is – incorrectly in this case – chosen to match the peak travel time of the data (simple
301 inspection of the breakthrough curve indicates a peak travel time of about 274 min), the
302 ADE solution is unable to capture the early arrivals and the long-time tailing (Fig. 3). In
303 this case, the mean velocity is approximately 6.0×10^{-3} cm/s, and the dispersion coefficient
304 was chosen to yield a breakthrough width similar to that using \bar{v}_w .

305 Finally, as an additional consideration, note that with a column length of 100 cm, the
306 peak travel time of 274 min can be translated to an overall assumed "mean" velocity of
307 about 6.1×10^{-3} cm/s, which is close to the estimate of $\bar{v}_T = 5.8 \times 10^{-3}$ cm/s from the
308 CTRW-PT simulation, and clearly distinct from the apparent mean water velocity $\bar{v}_w = 7.1$
309 $\times 10^{-3}$ cm/s. Moreover, from the same breakthrough curve, the velocity corresponding to
310 the time required for 50% of the tracer to be eluted from the column is essentially identical
311 to \bar{v}_T .

312

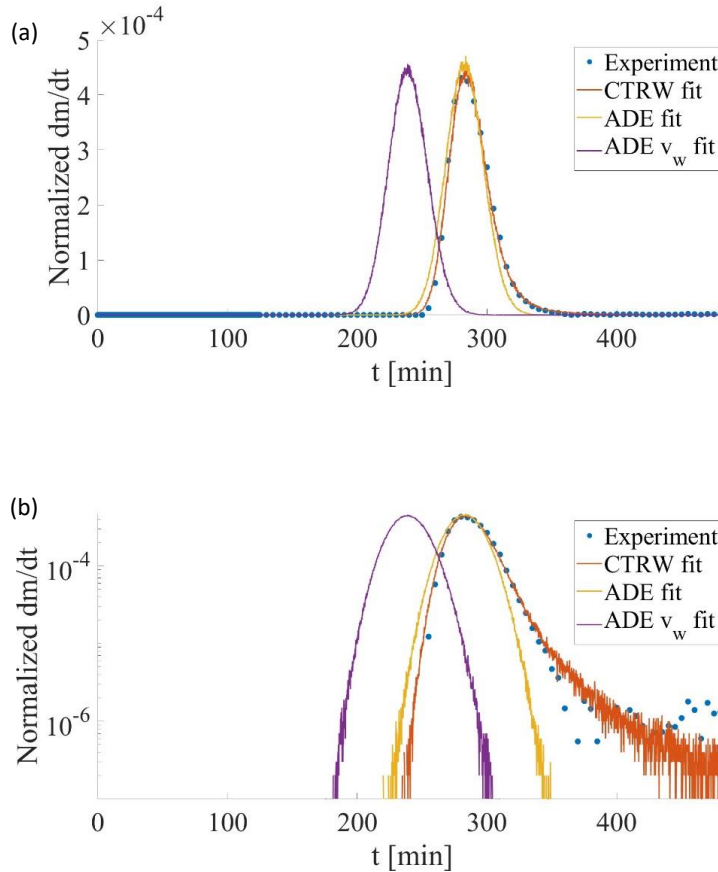


Figure 3. Comparison of experiment and CTRW simulation breakthrough curves for the D_2O slow flow homogeneous porous medium column (linear scale **(a)**). The long tails indicative of anomalous transport can be seen in the semi-log scale **(b)**, and in the modeled power law exponent ($\beta=1.84$). CTRW solution: $\bar{v}_T = 5.8 \times 10^{-3}$ cm/s (with a generalized dispersion coefficient of 0.14×10^{-3} cm²/s). Two solutions of the ADE are also shown, one using the value of $\bar{v}_w = 7.1 \times 10^{-3}$ cm/s (“ADE v_w fit”; with a dispersion coefficient of $D^* = 1.4 \times 10^{-3}$ cm²/s), and a fit to the peak of the data, yielding a velocity of 6.0×10^{-3} cm/s (“ADE fit”; with $D^* = 0.8 \times 10^{-3}$ cm²/s).

3.4 Implications of using isotopic waters for inferring catchment properties

The above analysis – for a macroscopically 1-D column – can be used to provide a first assessment of the impact of using differing estimates of a mean velocity on catchment



329 travel time estimates. It should be recognized at the outset that while catchments are
330 inherently complex, highly heterogeneous 3D systems, involving surface water, soil layer,
331 and aquifer components, catchment assessments are often based on largely 1D
332 conceptualizations, accounting for a *bulk* water and tracer input (recharge) region and an
333 ultimate discharge measured at a conveniently monitored outlet point (spring or stream)
334 (e.g., Stewart et al., 2010; Koeniger et al., 2010; Benettin et al., 2022; Rodriguez et al.,
335 2021).

336 In the column experiments discussed in Sect. 3.1, it was shown that water isotopes
337 migrate like inert tracers. Furthermore, it was shown in Sect. 3.3 that the tracer transport
338 displays non-Fickian behavior, with $\bar{v}_w \neq \bar{v}_T$ and longer-than-Fickian breakthrough tailing,
339 both of which affect the assessment of travel and residence times. In catchment assessment,
340 it is assumed that an often ambiguously defined mean travel time of water exists and that
341 it can be represented by considering a hydraulic retention time, which is defined as a
342 storage volume divided by a volumetric flow rate. Here, it is seen that the hydraulic
343 retention times are distinct from average residence times: one cannot observe the migration
344 of individual water molecules, but only the migration of tracers – whether inert chemicals
345 or water isotopes – in water. This implies that trapping of water isotopes in low conductive
346 regions will induce strong differences between estimated hydraulic retention times and
347 average isotope travel times.

348 Returning to the specific example calculation discussed in Sect. 3.3, mean travel times
349 over a 1 cm length are therefore ~140 s and ~172 s, for the apparent mean water velocity
350 ($\bar{v}_w = 7.1 \times 10^{-3}$ cm/s) and the mean tracer velocity ($\bar{v}_T = 5.8 \times 10^{-3}$ cm/s), respectively.
351 The mean particle transit time is longer than the water travel time due to the dispersion-
352 induced anomalous transport by a ratio of ~1.2, for these specific experiments.

353 Returning now to the background discussed in the Introduction, a key parameter of
354 interest in catchments is the assessment of the aquifer (fully water-saturated region) storage
355 thickness over an entire watershed; see, e.g., Stewart et al. (2010) for extensive discussion
356 of aquifer storage considerations. In this context, Stewart et al. (2010) provide an extensive
357 summary of published studies that report mean water isotope travel times in macroscale
358 catchments. The authors note that the various catchments appear sufficiently large to yield



359 relatively similar average behaviors. Moreover, the assessments all suggest the existence
360 of substantial storage volumes for recharge water into the aquifer zone.

361 These mean travel times estimates, which actually represent tracer transport and thus
362 \bar{v}_T , are all based on analysis of ^3H and assumed in these publications to represent the
363 apparent water velocity, \bar{v}_w . [It is recognized, parenthetically, that different isotopes are
364 likely to yield somewhat different average travel times, as may different inert chemical
365 tracers with different masses and rates of diffusion, but this factor is not relevant for the
366 key points and the short-term column experiments reported here.] If the tracer transport
367 were Fickian, then this estimate would indeed represent \bar{v}_T . However, real aquifers
368 generally display non-Fickian behavior (e.g., Goeppert et al., 2020; Dentz et al., 2023), and
369 in the example calculation given in Sect. 3.3, the true value of \bar{v}_w is a factor of ~ 1.2 faster
370 than \bar{v}_T . Stewart et al. (2010) conclude their analysis with an example calculation of a
371 catchment aquifer storage thickness, based on their summary of many catchments. They
372 posit a catchment with annual precipitation of 1000 mm, evapotranspiration of 600 mm
373 (and thus annual recharge of 400 mm/year), and 50% aquifer flow in a formation with an
374 overall porosity of 20%. For an estimated (apparent) mean (water) travel time of 10 years,
375 a 10 m aquifer thickness is needed over the entire watershed to account for the long travel
376 times in the data. However, given that water isotopes do not directly represent the water
377 mean travel times and yield longer travel times, the actual aquifer thickness may be lower.
378 The ratio of 1.2 between apparent mean water and mean tracer travel times calculated above
379 applies only to the specific columns studied here. However, applying the calculated ratio
380 for the scenario presented, to give a coarse estimate, would yield a significantly smaller
381 aquifer thickness of ~ 8 m. While the ratio of water and tracer mean travel times should be
382 estimated for any given scenario separately, the example above demonstrates the
383 importance of this estimation in inferring aquifer characteristics.

384

385 4 Conclusions

386 The experimental findings demonstrate the similarity between the measured transport
387 behavior of water isotopes and an inert chemical tracer in fully water-saturated porous
388 media. This similarity is evident across different flow velocities and porous medium



389 compositions. Notably, water isotopes exhibit the same transport behavior as tracers; the
390 very act of *tagging* water molecules, implicit in the measurement of any water isotope,
391 yields a measurement of their migration as a chemical tracer, which is not identical to the
392 bulk water flow. Moreover, the experiments here demonstrate that even in relatively
393 homogeneous sand columns, both water isotopes and inert chemical tracers exhibit non-
394 Fickian (anomalous) transport, and the mean tracer velocity is not necessarily equal to the
395 apparent mean water velocity. Consequently, studies that rely on water isotopes to estimate
396 catchment properties like water TTDs and aquifer storage thickness must recognize this
397 subtle but critical inequality between apparent mean water and mean tracer velocities, and
398 not use them interchangeably to represent the actual travel times of tracers and water
399 isotopes.

400

401 *Data availability.* The data on which this article is based are available online on Zenodo:
402 <https://zenodo.org/doi/10.5281/zenodo.12187848> (Elhanati et al., 2024).

403

404 *Competing interests.* At least one of the (co-)authors is a member of the editorial board of
405 Hydrology and Earth System Sciences. The authors have no other competing
406 interests to declare.

407

408 *Author contributions.* DE, EZ, ID, and BB formulated the ideas that resulted in the project,
409 defined the goals and aims of the study, and contributed to the various study components.
410 DE and BB developed the experimental methodology, ID and DE developed the isotope
411 analytical measurement protocol, and DE implemented the methodology and carried out
412 the data analysis. DE and BB drafted the initial manuscript. All authors took part in
413 reviewing and editing the final manuscript.

414

415 *Acknowledgments.* B.B. thanks the Minerva Foundation for support. D.E. gratefully
416 acknowledges the support of the Weizmann Institute for Environmental Sustainability.
417 B.B. holds the Sam Zuckerberg Professorial Chair in Hydrology.

418



419 *Financial support.* B.B. and E.Z. gratefully acknowledge support through the ViTamins
420 project, funded by the Volkswagen Foundation (Grant No. AZ 9B192).

421

422 **References**

423 Aquilina, L., Ladouche, B., and Dörfliger, N.: Water storage and transfer in the epikarst
424 of karstic systems during high flow periods, *J. Hydrol.*, 327, 472–485,
425 <https://doi.org/10.1016/j.jhydrol.2005.11.054>, 2006.

426 Benettin, P., Rodriguez, N. B., Sprenger, M., Kim, M., Klaus, J., Harman, C. J., van der
427 Velde, Y., Hrachowitz, M., Botter, G., McGuire, K. J., Kirchner, J. W., Rinaldo, A., and
428 McDonnell, J. J.: Transit time estimation in catchments: Recent developments and future
429 directions, *Water Resour. Res.*, 58, 1–36, <https://doi.org/10.1029/2022WR033096>, 2022.

430 Berkowitz, B., Cortis, A., Dentz, M., and Scher, H.: Modeling non-Fickian transport in
431 geological formations as a continuous time random walk, *Rev. Geophys.*, 44, 1–49,
432 <https://doi.org/10.1029/2005RG000178>, 2006.

433 Berkowitz, B., Dror, I., Hansen, S. K., and Scher, H.: Measurements and models of
434 reactive transport in geological media, *Rev. Geophys.*, 54, 930–986,
435 <https://doi.org/10.1002/2016RG000524>, 2016.

436 Berkowitz, B. and Zehe, E.: Surface water and groundwater: Unifying conceptualization
437 and quantification of the two “water worlds,” *Hydrol. Earth Syst. Sci.*, 24, 1831–1858,
438 <https://doi.org/10.5194/hess-24-1831-2020>, 2020.

439 Bijeljic, B., Mostaghimi, P., and Blunt, M. J.: Signature of non-Fickian solute transport in
440 complex heterogeneous porous media, *Phys. Rev. Lett.*, 107, 20, 204502.
441 <https://doi.org/10.1103/PhysRevLett.107.204502>, 2011.

442 Bijeljic, B., Raeini, A., Mostaghimi, P., and Blunt, M. J.: Predictions of non-Fickian
443 solute transport in different classes of porous media using direct simulation on pore-scale
444 images, *Phys. Rev. E*, 87, 013011, <https://doi.org/10.1103/PhysRevE.87.013011>, 2013.

445 Bowers, W. H., Mercer, J. J., Pleasants, M. S., and Williams, D. G.: A combination of
446 soil water extraction methods quantifies the isotopic mixing of waters held at separate



- 447 tensions in soil, *Hydrol. Earth Syst. Sci.*, 24, 4045–4060, <https://doi.org/10.5194/hess-24->
448 4045-2020, 2020.
- 449 Cortis, A., Chen, Y., Scher, H., and Berkowitz, B.: Quantitative characterization of pore-
450 scale disorder on transport in “homogeneous” granular media, *Phys. Rev. E.*, 70, 8,
451 <https://doi.org/10.1103/PhysRevE.70.041108>, 2004.
- 452 Dentz, M., Icardi, M., and Hidalgo, J.J.: Mechanisms of dispersion in a porous
453 medium. *J. Fluid Mech.*, 841, 851-882, <https://doi.org/10.1017/jfm.2018.120>, 2018.
- 454 Dentz, M., Kirchner, J. W., Zehe, E., and Berkowitz, B.: The role of anomalous transport
455 in long-term, stream water chemistry variability, *Geophys. Res. Lett.*, 50, 1–8,
456 <https://doi.org/10.1029/2023GL104207>, 2023.
- 457 Dentz, M., Scher, H., Holder, D., and Berkowitz, B.: Transport behavior of coupled
458 continuous-time random walks, *Phys. Rev. E*, 78, 1–9,
459 <https://doi.org/10.1103/PhysRevE.78.041110>, 2008.
- 460 Devell, L., Olin, Å., Dušek, K., and Klaban, J.: Measurements of the self-diffusion of
461 water in pure water, H₂O-D₂O mixtures and solutions of electrolytes,
462 <https://doi.org/10.3891/acta.chem.scand.16-2177>, 1962.
- 463 Edery, Y., Dror, I., Scher, H., and Berkowitz, B.: Anomalous reactive transport in porous
464 media: Experiments and modeling, *Phys. Rev. E*, 91, 1–13,
465 <https://doi.org/10.1103/PhysRevE.91.052130>, 2015.
- 466 Elhanati, D., Dror, I., and Berkowitz, B.: Impact of time-dependent velocity fields on the
467 continuum-scale transport of conservative chemicals, *Water Resour. Res.*, 59, 1–19,
468 <https://doi.org/10.1029/2023WR035266>, 2023.
- 469 Elhanati, D., Dror, I., Zehe, E., and Berkowitz, B.: Breakthrough curves of water isotopes
470 and inert chemical tracers through porous media columns [Data set], Zenodo,
471 <https://doi.org/10.5281/zenodo.12187848>, 2024.
- 472 Galbács, G., Kéri, A., Kálomista, I., Kovács-Széles, É., and Gornushkin, I. B.: Deuterium
473 analysis by inductively coupled plasma mass spectrometry using polyatomic species: An
474 experimental study supported by plasma chemistry modeling, *Anal. Chim. Acta*, 1104,



- 475 28–37, <https://doi.org/10.1016/j.aca.2020.01.011>, 2020.
- 476 Goeppert, N., Goldscheider, N., and Berkowitz, B.: Experimental and modeling evidence
477 of kilometer-scale anomalous tracer transport in an alpine karst aquifer, *Water Res.*, 178,
478 115755, <https://doi.org/10.1016/j.watres.2020.115755>, 2020.
- 479 Grathwohl, P., Rügner, H., Wöhling, T., Osenbrück, K., Schwientek, M., Gayler, S.,
480 Wollschläger, U., Selle, B., Pause, M., Delfs, J. O., Grzeschik, M., Weller, U., Ivanov,
481 M., Cirpka, O. A., Maier, U., Kuch, B., Nowak, W., Wulfmeyer, V., Warrach-Sagi, K.,
482 Streck, T., Attinger, S., Bilke, L., Dietrich, P., Fleckenstein, J. H., Kalbacher, T., Kolditz,
483 O., Rink, K., Samaniego, L., Vogel, H. J., Werban, U., and Teutsch, G.: Catchments as
484 reactors: A comprehensive approach for water fluxes and solute turnover, *Environ. Earth*
485 *Sci.*, 69, 317–333, <https://doi.org/10.1007/s12665-013-2281-7>, 2013.
- 486 Hrachowitz, M., Savenije, H., Bogaard, T. A., Tetzlaff, D., and Soulsby, C.: What can
487 flux tracking teach us about water age distribution patterns and their temporal dynamics?,
488 *Hydrol. Earth Syst. Sci.*, 17, 533–564, <https://doi.org/10.5194/hess-17-533-2013>, 2013.
- 489 Jury, W. A. and Sposito, G.: A transfer function model of solute transport through soil 1.
490 fundamental concepts, *Water Resour. Res.*, 22, 243–247, 1986.
- 491 Koeniger, P., Leibundgut, C., Link, T., and Marshall, J. D.: Stable isotopes applied as
492 water tracers in column and field studies, *Org. Geochem.*, 41, 31–40,
493 <https://doi.org/10.1016/j.orggeochem.2009.07.006>, 2010.
- 494 Lischeid, G., Lange, H., and Hauhs, M.: Information gain using single tracers under
495 steady state and transient flow conditions: the Gårdsjön G1 multiple tracer experiments,
496 in: *Tracers and modelling in hydrogeology. Proceedings of TraM’2000, the International*
497 *Conference on Tracers and Modelling in Hydrogeology held at Liège, Belgium, May*
498 *2000*, 73–77, 2000.
- 499 McDonnell, J. J. and Beven, K.: Debates - The future of hydrological sciences: A
500 (common) path forward? A call to action aimed at understanding velocities, celerities and
501 residence time distributions of the headwater hydrograph, *Water Resour. Res.*, 50, 5342–
502 5350, <https://doi.org/10.1002/2013WR015141>, 2014.



- 503 McDonnell, J. J., McGuire, K., Aggarwal, P., Beven, K. J., Biondi, D., Destouni, G.,
504 Dunn, S., James, A., Kirchner, J., Kraft, P., Lyon, S., Maloszewski, P., Newman, B.,
505 Pfister, L., Rinaldo, A., Rodhe, A., Sayama, T., Seibert, J., Solomon, K., Soulsby, C.,
506 Stewart, M., Tetzlaff, D., Tobin, C., Troch, P., Weiler, M., Western, A., Wörman, A., and
507 Wrede, S.: How old is streamwater? Open questions in catchment transit time
508 conceptualization, modelling and analysis, *Hydrol. Process.*, 24, 1745–1754,
509 <https://doi.org/10.1002/hyp.7796>, 2010.
- 510 McGlynn, B., McDonnell, J., Stewart, M., and Seibert, J.: On the relationships between
511 catchment scale and streamwater mean residence time, *Hydrol. Process.*, 17, 175–181,
512 <https://doi.org/10.1002/hyp.5085>, 2003.
- 513 McGuire, K. J. and McDonnell, J. J.: A review and evaluation of catchment transit time
514 modeling, *J. Hydrol.*, 330, 543–563, <https://doi.org/10.1016/j.jhydrol.2006.04.020>, 2006.
- 515 Nissan, A. and Berkowitz, B.: Reactive transport in heterogeneous porous media under
516 different Péclet numbers, *Water Resour. Res.*, 1–11,
517 <https://doi.org/10.1029/2019wr025585>, 2019.
- 518 Nissan, A., Dror, I., and Berkowitz, B.: Time-dependent velocity-field controls on
519 anomalous chemical transport in porous media, *Water Resour. Res.*, 53, 3760–3769,
520 <https://doi.org/10.1111/j.1752-1688.1969.tb04897.x>, 2017.
- 521 Rinaldo, A., Beven, K. J., Bertuzzo, E., Nicotina, L., Davies, J., Fiori, A., Russo, D., and
522 Botter, G.: Catchment travel time distributions and water flow in soils, *Water Resour.*
523 *Res.*, 47, 1–13, <https://doi.org/10.1029/2011WR010478>, 2011.
- 524 Rodriguez, N. B., Pfister, L., Zehe, E., and Klaus, J.: A comparison of catchment travel
525 times and storage deduced from deuterium and tritium tracers using StorAge Selection
526 functions, *Hydrol. Earth Syst. Sci.*, 25, 401–428, [https://doi.org/10.5194/hess-25-401-](https://doi.org/10.5194/hess-25-401-2021)
527 2021, 2021.
- 528 Simmons, C. S.: A stochastic-convective transport representation of dispersion in one-
529 dimensional porous media systems, *Water Resour. Res.*, 18, 1193–1214,
530 <https://doi.org/10.1029/WR018i004p01193>, 1982.



- 531 Sivapalan, M.: From engineering hydrology to earth system science: milestones in the
532 transformation of hydrologic science, *Hydrol. Earth Syst. Sci.*, 22, 1665–1693, 2018.
- 533 Sternagel, A., Loritz, R., Berkowitz, B., and Zehe, E.: Stepping beyond perfectly mixed
534 conditions in soil hydrological modelling using a Lagrangian approach, *Hydrol. Earth*
535 *Syst. Sci.*, 26, 1615–1629, <https://doi.org/10.5194/hess-26-1615-2022>, 2022.
- 536 Sternagel, A., Loritz, R., Klaus, J., Berkowitz, B., and Zehe, E.: Simulation of reactive
537 solute transport in the critical zone: A Lagrangian model for transient flow and
538 preferential transport, *Hydrol. Earth Syst. Sci.*, 25, 1483–1508,
539 <https://doi.org/10.5194/hess-25-1483-2021>, 2021.
- 540 Stewart, M. K., Morgenstern, U., and McDonnell, J. J.: Truncation of stream residence
541 time: How the use of stable isotopes has skewed our concept of streamwater age and
542 origin, *Hydrol. Process.*, 24, 1646–1659, <https://doi.org/10.1002/hyp.7576>, 2010.
- 543 Weiler, M., McGlynn, B. L., McGuire, K. J., and McDonnell, J. J.: How does rainfall
544 become runoff? A combined tracer and runoff transfer function approach, *Water Resour.*
545 *Res.*, 39, 1–13, <https://doi.org/10.1029/2003WR002331>, 2003.
- 546 Wienhoefer, J., Germer, K., Lindenmaier, F., Farber, A., and Zehe, E.: Applied tracers for
547 the observation of subsurface stormflow at the hillslope scale, *Hydrol. Earth Syst. Sci.*,
548 13, 1145–1161, <https://doi.org/10.5194/hess-13-1145-2009>, 2009.
- 549